3D ROAD-MARK RECONSTRUCTION FROM MULTIPLE CALIBRATED AERIAL IMAGES

Olivier Tournaire[1,2], Nicolas Paparoditis[1], Franck Jung[3], Bernard Cervelle[2]

[1]IGN / MATIS, 2-4, Ave Pasteur, 94165 S^t-Mandé - France
[2]UMLV, 5, Bd Descartes, Champs-sur-Marne 77454 Marne-la-Vallée CEDEX 2 - France
[3]ESGT, 1, Bd Pythagore, 72000 Le Mans - France

{olivier.tournaire;nicolas.paparoditis}@ign.fr franck.jung@esgt.cnam.fr bernard.cervelle@univ-mlv.fr

KEY WORDS: 3D reconstruction, Road-marks, Object extraction, Template matching, Correlation, Hierarchical estimation

ABSTRACT:

A method for accurate 3D reconstruction of road features from multiple calibrated aerial images of urban areas is proposed in this paper. We here focus on road-marks and in particular on zebra-crossings and discontinuous road-marks separating circulation lanes. The approaches used here are generic and based on a-priori external knowledge and thus constrain the extraction of image features. As we will explain, two strategies are adopted depending on the object size. For zebra-crossings, we first build 3D segments representing stripes' borders by 2D segments matching. For discontinuous lanes, we build a graph describing the network in each image and then match nodes in order to obtain 3D position of stripes' centers. This provides in both cases an initial solution in 3D space. Using geometric and radiometric modeling to obtain a set of plausible models, e then look for an optimal solution. The last step yields us to choose the best one in adequacy with images data. A correlation based energy and template matching strategy achieve this in a hierarchical frame. The algorithm is finally evaluated with ground control points surveyed with a millimetric precision.

1 INTRODUCTION

Most of the photogrammetric research on object extraction from aerial images in the last years has focused on building reconstruction. However, the road network is extremely structuring for urban scene analysis and for defining possible building ROIs. In addition, in 3D city models, roads and pavements should need to be described as well as buildings, thus needing a surfacic representation and a decimetric and geometric accuracy instead of the classical linear spaghetti model encountered in most of Road GIS databases. In this scope, (Vosselman, 2003) proposed a 3D road reconstruction from LASER points cloud and a cadastral map. For these applications, road-marks are very interesting descriptors of the road surface architecture. Semantic and functional informations can be derived from them: way of circulation, number of lanes, special lanes (public transport, ...). They can be used in numerous applications such as cartographic road databases updating (Zhang, 2003), road extraction (Hinz and Baumgartner, 2002; Steger et al., 1997) or creation of visual landmarks used in autonomous navigation systems (Royer et al., 2006).
Concerning ground-based imagery, many papers were published and various approaches are used. (Se and Brady, 2003) detect zebra-crossings for outdoor aid navigation for the partially sighted using vanishing lines. (Rebut et al., 2004) proposed a method for road marks analysis with mathematical morphology and a training database. For an automatic road marking repainting tool, (Charbonnier et al., 1997) designed an algorithm analysing segments by pairs. In real time driver assistance (Enkelmann et al., 1995) introduced a method using parallel segments and radiometric features in order to detect marking lanes.
The link between aerial and terrestrial imagery has become more and more important in the last years. It is crucial for instance for urban environments reconstruction problematics such as georeferencing and / or matching of images produced by mobile mapping systems (MMS) or to texture 3D models obtained from aerial imagery (Pénard et al., 2006). Most of the problems encountered by MMS lies in the fine and robust absolute localisation of the vehicle. Direct georeferencing methods such as GPS combined with INS and / or other sensors (odometers, gyroscopes, ...) are often used. However, in dense urban areas, GPS masks, multi-path errors and bad satellites configurations are extremely frequent. These errors cannot be fully corrected with an INS due to its relative drift on long distances providing an absolute accuracy from 0.5 m to 1 m. Thus, to provide an accurate georeferencing, we have to deal with external data to introduce constraints on the position. A strategy is to integrate in the system aerial images georeferenced with a bundle adjustement. Images then become the key-frame for obtaining absolute localisation by matching shapes detected from the two points of view.
In France, zebra-crossings, and more generally road marks are (in most cases) governed by careful specifications[1]. Moreover, these kinds of objects can be considered as invariants with a simple shape not suffering from generalisation, e.g to match aerial and ground based images or for the generation of landmarks databases for autonomous navigation.
This paper describes robust and accurate road-mark detection and reconstruction experts that can be helpfull for all previously described applications. We will not at all describe the reconstruction of the road network topology which could be in any case be extracted from medium-scale existing databases (at least in Europe and North America) but only describe two road-mark experts that could be helpfull to derive higher level information in a more complete system. The paper is organised as follows. A first part presents the algorithm for 3D zebra-crossing reconstruction. A second one is focused on the 3D reconstruction of dashed lanes. We then present in a third section a hierarchical method for refining the 3D position of the detected objects. Finally, we present briefly numerical results and evaluations.

2 ZEBRA-CROSSING RECONSTRUCTION

We first choose to reconstruct zebra-crossings because they strongly structure the road network in urban areas. Moreover, they are the

[1]Source: Ministère de l'Intérieur et Ministère de l'Equipement, de l'Aménagement du Territoire et des Transports: *Instruction interministérielle sur la signalisation routière*. 1988.

objects covering the greatest surface.

2.1 Zebra-crossing specifications

The specifications show that pedestrian walkaways have a fixed width of 0.5 m. The length of each stripe is only described in urban areas by a minimal size of 2.5 m. Two consecutive stripes are separated by a distance in the range $[0.5m; 0.8m]$, but is regular for a zebra-crossing. Finally, the stripes are white on a black background, but in special cases, like pedestrian areas, the hue can be inversed, or the background can be colored. Zebra-crossings have most of the time four to twenty stripes, and their maximum length is around 6 m.

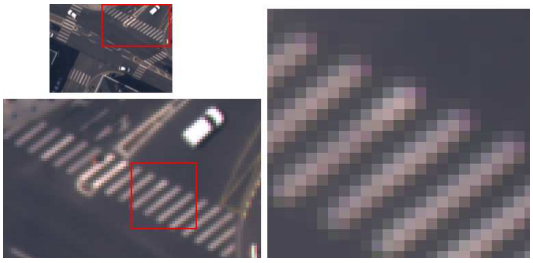

Figure 1: Extracts of a 4000×4000 digital image in Amiens (25 cm ground pixel)

2.2 Zebra-crossing extraction

Our strategy relies on 2D segments lines image features. We use the Canny-Deriche edge detector (Deriche, 1987). The images are oversampled by a factor 2 to have a better sampling of the convolution filter, and α is set to 1.5 to handle a compromise between localisation and sensitivity to noise. A hysteresis threshold is then processed, followed by subpixelar localisation of each contour point. Finally, chaining of contour points and polygonalisation is performed by the Douglas-Peucker algorithm (Douglas and Peucker, 1973). We now have 2D segments, with the knowledge of their covariance matrix in (ρ, θ) polar coordinates (Deriche et al., 1991).
In order to find zebra-crossings' segments, we analyse their relative organisation, and use specifications. First, segments are filtered on their length, taking in account a tolerance error. After this, we search for parallel groups of segments (with a tolerance taking in account the angular variance) respecting stripes size and distance between stripes. The homogeneity of length is equally computed, thus following again specifications. Finally, we retain objects that have at least six segments.

2.3 3D segments reconstruction

This 2D processing provides a set of segments belonging to zebra-crossings. We now build 3D segments with the detected structures in the images. For 3D segments reconstruction, we choose a true multi-image matching algorithm of sweep-planes (Collins, 1996) (more details can be found in (Taillandier, 2004)). Here, we introduce an external data - a DSM computed by image matching (Pierrot-Deseilligny and Paparoditis, 1996) - to limit search space to cut down combinatory. The DSM is morphologically dilated (to define an upper and lower bounding surface) and the object space is discretised in voxels. The sweep step and the cells' size are defined with respect to the flight parameters.
With this sweep-plane technique, we obtain for each voxel segments correspondences between each images. To reconstruct a 3D segment from a match, we use a two step minimisation procedure. We first construct a set of 3D segments by intersecting two by two all the pairs of planes within the set (see Figure 2 and 3). Each plane is defined by the center of projection of the camera and goes through the image straight line. Each segment of a set defines a $(P_i, \overrightarrow{u_i})$ 3D line. The final 3D segment lies on the line whose direction $\overrightarrow{v}$ minimises in a robust way the sum of angular difference with all the segments of a given set (see Equation 1). Using a least squares minimisation, it leads to find the vector $X = \overrightarrow{v} = (x, y, z)^t$ by solving the system $A^tAX = 0$ where A^tA is the 3×3 matrix defined in Equation 2. Vector X is finally obtained by extracting the eigenvector corresponding to the smallest eigenvalue of A^tA. Note that the normalisation of the $\overrightarrow{u_i}$ leads to the constraint $\|X\| = 1$.

$$\underset{\overrightarrow{v}}{argmin} \sum_i \sin^2(\overrightarrow{v}, \overrightarrow{u_i}) \equiv \underset{\overrightarrow{v}}{argmin} \sum_i \left\| \overrightarrow{v} \wedge \overrightarrow{u_i} \right\| \quad (1)$$

$$A^tA = \begin{pmatrix} \sum_i (u_{i_y}^2 + u_{i_z}^2) & -\sum_i u_{i_x} u_{i_y} & -\sum_i u_{i_x} u_{i_z} \\ -\sum_i u_{i_x} u_{i_y} & \sum_i (u_{i_x}^2 + u_{i_z}^2) & -\sum_i u_{i_y} u_{i_z} \\ -\sum_i u_{i_x} u_{i_z} & -\sum_i u_{i_y} u_{i_z} & \sum_i (u_{i_x}^2 + u_{i_y}^2) \end{pmatrix} \quad (2)$$

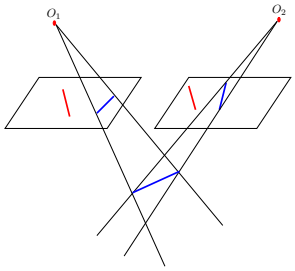

Figure 2: One possible two by two planes intersection

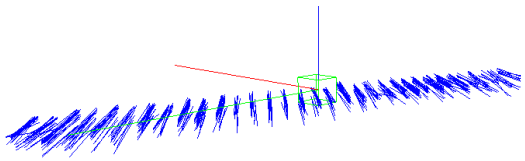

Figure 3: Zebra-crossing of Figure 1 3D segments corresponding to the two by two intersection of pairs of planes

Once we have the direction, we have to find the point which the 3D line goes through. It is defined as the one which minimises the sum of distances to each 3D segment of a given set. Using the same techniques, we have to solve the system $A^tAX = B$ where B is a 3×1 vector. Finally, the end-points of the reconstructed 3D segment are given by projecting orthogonally the extremities of each segment of the considered set and computing the union (see Figure 4 - (Xu and Z.Zhang, 1996)).

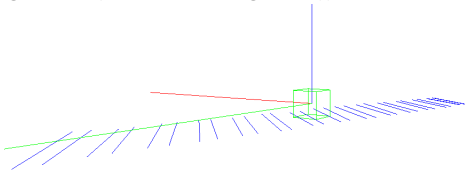

Figure 4: Final 3D segments

This process only reconstructs the long sides of the stripes. We now need to find the transversal axis , i.e the stripes' small side. Thus, we have to find two 3D lines, each of this corresponding to one transversal side of the zebra-crossing. On each side of it, we use a robust least squares minimisation on the long side segment

extremities to find those 3D lines. The small sides are then obtained by projecting those lines on the stripes' borders segments. To find a stripe, and thus know which borders we have to link two by two, we use the gradient direction and distance between two consecutive segments (distances constraints from specifications are introduced). Result is shown on Figure 5.

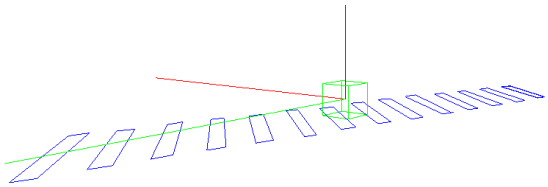

Figure 5: Final zebra-crossing stripes of Figure 1

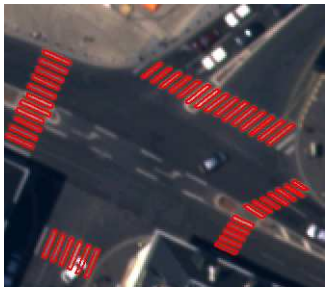

Figure 6: Final zebra-crossings projected in image space

Each stripe of a zebra-crossing is now modeled by a 3D parallelogram and is considered as an initial solution for a fine position refinement described in section 4

3 DISCONTINUOUS ROAD-MARKS RECONSTRUCTION

The other road-mark feature extremely structuring for the road network is the discontinuous line. We now present our strategy for its reconstruction.

3.1 Discontinuous road-marks specifications

Many kind of Discontinuous Road-Marks (DRM) can be found in urban environments. They depend on the road functionality, or on the road type, and the stripes they are composed of are defined by three characteristics: the length, the width and the distance between consecutive stripes. Table 1 and Figure 7 give an overview of the discontinuous road-marks available in the French towns.

Type	Stripes length (m.)	Distance between stripes (m.)
T3	3	1.33
T2	3	3.5
T'2	1.33	5

Table 1: Specifications for discontinuous road-marks

3.2 Monocular extraction

We do not use the protocol presented for zebra-crossing. DRM are objects whose size is under the ground pixel size. Indeed, their stripes are at most 12 cm width. So, working directly with segments in 3D space is not possible because these image features at this resolution are highly miss located: the stripes' borders are stretch toward the exterior, and because of their small length, segments lines have also a very noisy direction. So, the protocol described in 2.3 will be inefficient for reconstructing 3D segments

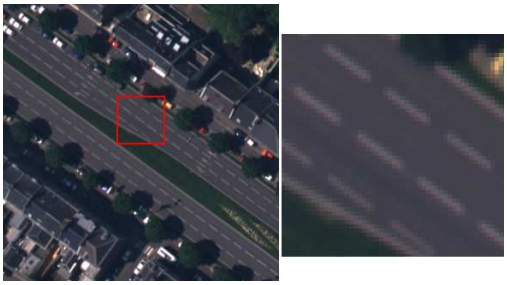

Figure 7: Extracts of a 4000×4000 digital image in Amiens (25 cm ground pixel)

describing stripes' borders. A graph representation - which provides the neighbors of an object - is for this purpose more robust, because predecessor and successor of a stripe will provide a fine orientation needed for the 3D reconstruction of stripes' borders.
The strategy for DRM detection is based on graph theory. The graph construction of the DRM in an image consists in finding arrangements of segments who best fit the external geometric knowledge from specifications. As for zebra-crossings, segments are extracted and we only keep the ones belonging to a specific length interval defined by the type of DRM we want to extract (see Table 1). We then have segments that potentially belong to DRM. We now have to describe arrangements between those road-marks. So, we build numerical potentials describing the strength of the interactions between pairs of segments. Three potentials described below are used in our application: a connection potential, an alignment potential and a potential for the the length homogeneity. The value for each potential is given by a set of parameters and takes a value thanks to a function.

3.2.1 Potential function

The potential function ζ is generic and has the same general shape for each potential. Two parameters describe it (c and e). However, this function must respect a set of constraints:

- its values must be in $[0;1]$
- it must be symmetric
- it must be increasing on $[-1;0]$
- $\begin{cases} \zeta(c) = \zeta(-c) = 0 \\ \zeta(0) = 1 \\ \forall x \in [-e;e]\,, \zeta(x) = 1 \end{cases}$

The symmetry is important because angles are computed on $[0;2\pi]$. The parameter c allows to choose the extension of the potential function. e is used to have a "plateau" defining a set of values for which the potential function takes its maximum value. Finally, we choose to define the function ζ as:

$$\begin{array}{ccccc} \zeta & : & \mathbb{R}^3 & \rightarrow & [0;1] \\ & & \begin{pmatrix} x \\ c \\ e \end{pmatrix} & \mapsto & \begin{cases} 1 & \text{if} & |x| \leq e \\ 0 & \text{if} & |x| \geq c \\ \frac{c^2-x^2}{c^2-e^2} & \text{else} & \end{cases} \end{array} \tag{3}$$

3.2.2 Potentials definitions

Connection potential

This is the first potential to be computed because if it is null, the others are undefined. Around a given segment s_i, we define a region of interest $ROI_{s_i} = ROI_{s_i}^{(1)} \cup ROI_{s_i}^{(2)}$. Given an angular tolerance θ_c, $ROI_{s_i}^{(j)}$ is an union of discs of radii r_c located at a given distance from $\overline{s_i}$ the middle of s_i in the direction of s_i. This surface is approximated by a trapeze (see Figure 8).
We then look for segments s_j whose middle $\overline{s_j}$ belongs to ROI_{s_i}. If such segments exist, the connection potential is:

$$\mathcal{P}(s_i \underset{c}{\sim} s_j) = \zeta\big(d(\overline{s_i}, \overline{s_j}) - d_{th}, c_c, e_c\big) \tag{4}$$

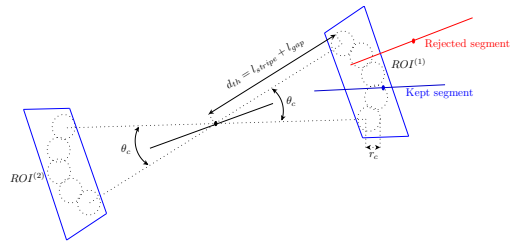

Figure 8: Connection potential description

where d_{th} is the distance between two consecutive stripes. c_c can be defined as a fraction of d_{th} and e_c allows to take into account segment detection accuracy.

Alignment potential

After the connection potential, we compute an alignment potential. It is an angular difference between the two segments s_i and s_j we are studying. The angular difference θ_i^j is then $\theta_i^j = \theta_i - \theta_j$ (see Figure 9). As we want to penalise pairs of segments having a high angular difference, the alignment potential is:

$$\mathcal{P}(s_i \underset{a}{\sim} s_j) = \zeta\left(\theta_i^j, c_e, e_a\right) \tag{5}$$

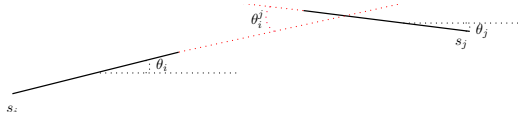

Figure 9: Alignment potential description

In our application, we use $c_e = \pi/2$ because when segments are perpendicular, the potential must be null. e_a is set to avoid penalising curved roads, and can take into account the segment's variance, i.e uncertainties on their angular parameter.

Length potential

This potential is useful to know the length homogeneity of two segments s_i and s_j. We assign a higher potential to pairs of segments of the same length - in a DRM network stripes have the same length (see Figure 10). Thus, we compute the norms' ratio:

$$\mathcal{P}(s_i \underset{l}{\sim} s_j) = \zeta\left(1 - \min\left(\frac{\|s_i\|}{\|s_j\|}, \frac{\|s_j\|}{\|s_i\|}\right), c_l, e_l\right) \tag{6}$$

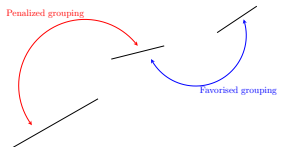

Figure 10: Length homogeneity potential description

e_l allows to have a tolerance on the length. Indeed, the edge detector is very sensitive and often, segments are truncated at their extremities. This parameter is then set to take this observation into account, and so on to avoid penalising grouping of pairs of segments having a small length difference. In addition, we use $c_l = 1$.

Global potential

Finally, once we have computed the three individual potentials, we use a global potential to summarise existing relations between pairs of segments. The global potential is simply a weighted sum:

$$\begin{cases} \mathcal{P}(s_i \underset{G}{\sim} s_j) = \sum\limits_{k=c,a,l} \alpha_k \mathcal{P}(s_i \underset{k}{\sim} s_j) \\ \forall k, \alpha_k \geq 0, \sum\limits_k \alpha_k = 1 \end{cases} \tag{7}$$

As we know, there is a high incertitude on segments norms, so α_l is the smallest coefficient. In addition, α_c and α_a are high, and can be equivalent, but most of the time, we will have $\alpha_c > \alpha_a$. In our application, we often use $\alpha_c = 0.45$, $\alpha_a = 0.35$ and $\alpha_l = 0.2$

To be sure to find the objects relations we are looking for, we use a threshold δ_k on each individual potential and also on the global one. Thus, two segments s_i and s_j are considered to be in interaction, only if the following conditions are respected:

$$\begin{cases} \forall k \in \{c, a, l\}, \mathcal{P}(s_i \underset{k}{\sim} s_j) > \delta_k \\ \mathcal{P}(s_i \underset{G}{\sim} s_j) > \delta_G \end{cases} \tag{8}$$

It is efficient to obtain good results and also in terms of time consuming. Interactions are stored in an $n \times n$ adjacency matrix, where n is the number of selected segments. A segment is selected only if it interacts with another one. The matrix fully describes our DRM network, but we need some simplifications in order to obtain a graph composed of nodes and edges.

Note that some tests show that α_k and δ_k values are not critical.

3.3 Graph creation

As we used a segment detector for our modeling of DRM network, a stripe is most of the time composed of two parallel segments. We want to have a node representing each stripe, and a valued edge (modeling interaction's strength) linking two adjacent stripes.

Thus, a node is created with the following rules:

- if there is only one segment for a stripe, the node is its middle,
- if there are two segments for a stripe, the node is the barycenter of the four extremities (a stripe is composed of two segments if two segments having the same direction and a high recovering are found in a small neighborhood)

The valuations between two edges are computed using the interactions values between pairs of segments composing each stripe. Thus, if we consider two stripes (i.e two nodes), the valuation of the edge linking them is the maximum of the interaction between their segments.

As we use 2D noisy segments lines, the center of a stripe as computed above can only be considered as an estimation of the real position. To obtain a best solution, we build a 2D radiometric template (see section 4) with the known geometry and find the best location of the center by moving the template in the vicinity of the node and optimising a similarity score.

3.4 Chaining road-marks

The graph created in 3.3 is used to extract DRM chains. This is done recursively on its adjacency matrix. We search for long paths and validate them with geometric characteristics. We first look for regularity, i.e a path must not be auto-intersecting and its curvature must vary slowly. In addition, some structures are found on the roofs (false alarms). We filter them using a DTM generated from a DSM. Results are shown on Figure 11.

3.5 3D Reconstruction

A graph of the DRM is created as described in the previous sections for each images. The last step of the reconstruction process consists in matching nodes across the different views. We use here a simple algorithm consisting in making each image being successively the master one. For each stereopairs and epipolar constraints, we search for candidates for matching. The graph structure allows introducing topological, i.e neighborhood constraints. We can thus create a set of possible matches.

From each matching possibility, a 3D point is reconstructed by intersecting the rays (a ray is a 3D line going through the camera's center of projection and the image point). The resulting 3D point

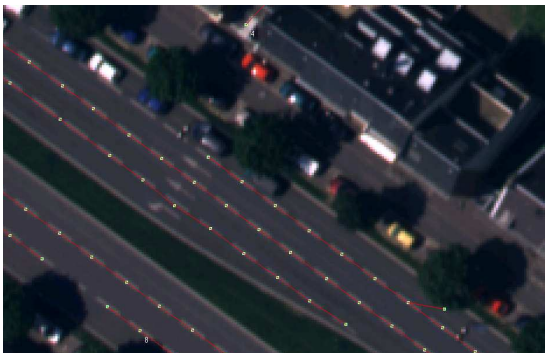

Figure 11: Road marks chaining

is the one which minimises the sum of distances to the rays. To decide between concurrent matches, we use a DSM and check for the Z difference between the reconstructed point and the height given by the DSM. A multi-image similarity score is also used to validate or not the 3D point.
We thus obtain 3D points describing the center of DRM's stripes. Note that if an object (car, tree, ...) hides a DRM element in an image, the multi-image frame allows to obtain with this robust 3D reconstruction the missing element if it is at least not occluded in two images. A 3D reconstruction is given on Figure 12.

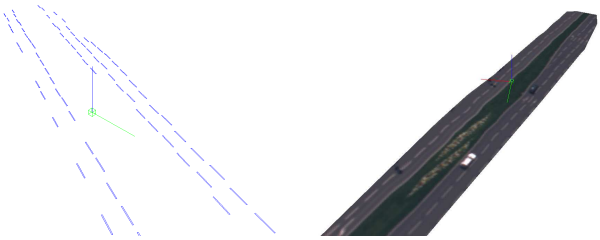

Figure 12: 3D DRM reconstruction and textured triangulation on the 3D stripes' centers

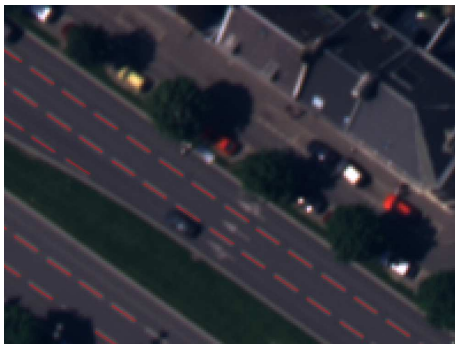

Figure 13: Final DRM of Figure 12 projected on image space

4 3D OBJECTS POSITION REFINEMENT

The strategies presented in 2.2 and 3.2 provides us a robust initial solution that needs to be refined. So, we model a stripe as a parallelogram in 3D space and try to find its optimal position using multiple images (Baltsavias, 1991) in a hierarchical frame. The idea is to distort the base model (the initial solution) in 3D space and to correlate a derivated 2D signal with images data. (Jain et al., 1996) uses this principle in 2D space with a grid transformation. An other modeling of this strategy is proposed in (Chen et al., 2003).

4.1 Notations and definitions

$\mathcal{M}_r^{(n)}$: the model of reference at level n (see 4.3),
$\mathcal{M}_b$: the best model,
$\mathcal{T}$: a class of transformations,
T_i: a transformation ($\mathcal{T} = \bigcup_i T_i$),
$\mathcal{M}_i$: a transformed model ($\mathcal{M}_i = T_i \mathcal{M}_r^{(n)}$).

An object's model is represented with a set of four points. So, a model is defined by the central point $p_i = (x_i, y_i)^t$ of the stripe, its length L_i and direction d_i^1, its width l_i and direction d_i^2.
A transformation is the set of operations used for the generation of the model hypothesis. Both for zebra-crossing and DRM stripe, it is composed of two rotations $\widetilde{r_1}$ and $\widetilde{r_2}$ along the directions vectors d_i^1 and d_i^2, and of translations t_1, t_2 and t_3 along each 3D axis. Specially for zebra-crossings, the transformations also have to take into account the length and width variations of the object. Finally, a model is composed of five parameters for a DRM stripe and of six parameters for a zebra-crossing stripe (see Equation 9).

$$\begin{cases} T_i^{Zebra}(\widetilde{r_1}, \widetilde{r_2}, t_1 \vec{X}, t_2 \vec{Y}, t_3 \vec{Z}, \alpha L_i) = T_i^{Zebra}. \\ T_i^{DRM}(\widetilde{r_1}, \widetilde{r_2}, t_1 \vec{X}, t_2 \vec{Y}, t_3 \vec{Z}) = T_i^{DRM}. \end{cases} \quad (9)$$

The vectors of parameters to be estimated are then defined by:

$$\begin{cases} \Theta^{Zebra} = (\widetilde{r_1}, \widetilde{r_2}, t_1, t_2, t_3, \alpha) \\ \Theta^{DRM} = (\widetilde{r_1}, \widetilde{r_2}, t_1, t_2, t_3) \end{cases} \quad (10)$$

4.2 Model choice

To choose the best 3D position for a stripe, our strategy is to compare the image signal with a perfect simulated signal. For each model in 3D space $\mathcal{M}_i$ we have four points making a parallelogram. The knowledge of the projection geometry allows to project this shape in all the images I_j. We thus obtain for each vertex of $\mathcal{M}_i$ its subpixellar position in 2D images spaces. We then simulate a signal SS_{ij} (j stands for the image number) with this positions for each images, i.e a white anti-aliased 2D shape on black background. Finally, the best 3D model $\mathcal{M}_b$ is chosen by maximising the following energy:

$$\mathcal{M}_b = \max_i \sum_j Corr_{\mathcal{M}_i}(SS_{ij}, I_j) \quad (11)$$

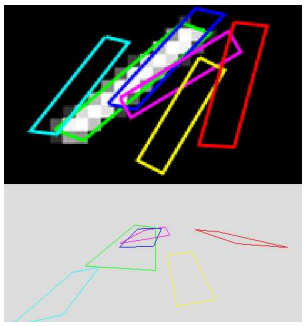

Figure 14: Projections in image space of 3D models (lower image) on a simulated signal (upper image). Each color corresponds to a different model $\mathcal{M}_i$. The found solution is in green.

4.3 Hierarchical models generation

As we have six parameters to estimate a zebra stripe and five for a DRM stripe, the computational search space is huge (because all parameters are estimated simultaneously) and need to be reduced. That is why we adopt an iterative multi-scale frame (Kropatsch, 1991; Hummel, 1988). For each level of the hierarchy, we set search spaces and steps. This idea has already been used in different context (Gharavi-Alkhansari, 2001; Stefano et al., 2005).
The system is initialised with $\mathcal{M}_r^{(n)}$ (the initial solution). At this level n of the hierarchy, the search spaces and sampling distances on the parameters are the biggest. From this reference model and with a class of transformations $\mathcal{T}$, we build several models $\mathcal{M}_i$ and the simulated SS_{ij} signals in the images. Then, the best model $\mathcal{M}_b^{(n)}$ at this level is given by Equation 11. We go down a level of the hierarchy and repeat this process with initialising $\mathcal{M}_r^{(n-1)}$ with $\mathcal{M}_b^{(n)}$.
Each time we go down a level, the search spaces and sampling distances are reduced. Here, for both we use a dyadic factor. This protocol is iterated while $n > 0$ or convergence is reached.
The number n of levels of the hierarchy, the search spaces and sampling distances are chose to be in adequation with the wished accuracy for the final stripe position.

5 RESULTS

To test the robustness of our algorithms and their ability to detect and reconstruct road marks, we have a reference database of points surveyed with a millimetric accuracy on the town of Amiens. It is composed of both zebra-crossings and DRM stripes' corners, and were acquired with classical topometric techniques. The evaluations were done only for the zebra-crossings, but give clear information about the algorithm's accuracy. $\frac{B}{H}$ ratio is in the range $[0.2; 0.6]$ and reconstructions were performed using from 3 to 9 images. We first measure absolute planimetric and altimetric accuracies on a set of 112 stripes. The RMS is about 15 cm for the first one, and less than 20 cm for the second one mainly to the quality of the aerial triangulation. In terms of relative accuracy, the algorithm shows its ability to be very fine. Indeed, it's about only a few cm, meaning that the global structure of a zebra-crossing is preserved by our algorithm. We can also note that the geometric refining presented in section 4 gives good results. The accuracy gain is about 5 cm. For both zebra-crossing and DRM, there are only a few false positives alarms because there are no ground structures having the same radiometric and geometric properties as the objects we want to reconstruct. In addition, the false positives detected for DRM are located on the buildings' roof and can easily be filtered with a focalisation mask. However, the detection rate is higher than 90% for zebra-crossing stripes. The missing stripes are the small ones located near the pavement, the ones hidden by a car or the old ones degraded (thus loosing their geometric and radiometric properties).

6 CONCLUSION AND FUTURE WORKS

As we have shown on examples, our modeling and detection of the road-marks is very efficient for road detection and characterisation in an urban environment. In can also be extended to suburban areas or motorways.
To obtain a tool able to give more complete informations on the road network, we now have to detect other road-marks (specialised lanes, bus stops, traffic informations, ...).
An other key point to take advantage of our systems (aerial and terrestrial) is to have a full collaboration between them, e.g to search for missing objects in the images from the other viewpoint. We have presented 3D reconstructing experts for road marks which are a structuring features of the road network e.g to separate lanes and estimate their width.

REFERENCES

Baltsavias, E., 1991. Multiphoto geometrically constrained matching. PhD thesis, Institute for Geodesy and Photogrammetry, ETH Zurich.

Charbonnier, P., Diebolt, F., Guillard, Y. and Peyret, F., 1997. Road markings recognition using image processing. In: IEEE Conference on Intelligent Transportation System, Vol. 1, pp. 912–917.

Chen, J. H., Chen, C. S. and Chen, Y. S., 2003. Fast algorithm for robust template matching with M-estimators. In: IEEE Transactions on Signal Processing, Vol. 51-1, pp. 230–243.

Collins, R., 1996. A sweep-space approach to true multi-image matching. In: Proceedings of the 15^{th} Conference on Computer Vision and Pattern Recognition, San Francisco - USA.

Deriche, R., 1987. Using Canny's criteria to derive a recursively implemented optimal edge detector. International Journal of Computer Vision 1(2), pp. 167–187.

Deriche, R., Vaillant, O. and Faugeras, O., 1991. From noisy edge points to 3D reconstruction of a scene: a robust approach and its uncertainty analysis. In: Proceedings of the 7^{th} Scandinavian Conference on Image Analysis, Alborg - Danmark, pp. 225–232.

Douglas, D. H. and Peucker, T. K., 1973. Algorithms for the reduction of the number of points required to represent a digitized line or its caricature. The Canadian Cartographer 10(2), pp. 112–122.

Enkelmann, W., Struck, G. and Geisler, J., 1995. ROMA - a system for model-based analysis of road markings. In: IEEE Proceedings of the Intelligent Vehicle '95 Symposium, Vol. 1, Graz - Austria, pp. 356–360.

Gharavi-Alkhansari, M., 2001. A fast globally optimal algorithm for template matching using low-resolution pruning. IEEE Transactions on Image Processing 10(4), pp. 526–533.

Hinz, S. and Baumgartner, A., 2002. Urban road net extraction integrating internal evaluation model. In: ISPRS Commission III Symposium on Photogrammetric Computer Vision, Vol. XXXIV - Part 3A, Graz, Austria, pp. 163–168.

Hummel, R., 1988. The scale-space formulation of pyramid data structures. Parallel Computer Vision pp. 107–123.

Jain, A. K., Zhong, Y. and Lakshmanan, S., 1996. Object matching using deformable templates. IEEE Transactions on Pattern Analysis and Machine Intelligence 18(3), pp. 267–278.

Kropatsch, W., 1991. Image pyramids and curves, an overview.

Pénard, L., Paparoditis, N. and Pierrot-Deseilligny, M., 2006. Reconstruction 3D automatique de façades de bâtiments en multi-vues. In: RFIA, Tours - France.

Pierrot-Deseilligny, M. and Paparoditis, N., 1996. A multiresolution and optimization-based image matching approach: an application to surface reconstruction from SPOT5-HRS stereo imagery. In: WG I/5-6 Workshop on Topographic Mapping from Space, Vol. XXXVI, Ankara - Turkey.

Rebut, J., Bensrhair, A. and Toulminet, G., 2004. Image segmentation and pattern recognition for road marking analysis. In: IEEE International Symposium on Industrial Electronics, Vol. 1, Graz - Austria, pp. 727–732.

Royer, E., Lhuillier, M., Dhome, M. and Lavest, J.-M., 2006. Localisation par vision monoculaire pour la navigation autonome: précision and stabilité de la méthode. In: RFIA, Tours - France.

Se, S. and Brady, M., 2003. Road feature detection and estimation. Machine Vision and Applications 14(3), pp. 157–165.

Stefano, L. D., Mattoccia, S. and Mola, M., 2005. An efficient algorithm for exhaustive template matching based on normalized cross correlation. In: Proceedings of the 12^{th} International Conference on Image Analysis and Processing.

Steger, C., Mayer, H. and Radig, B., 1997. The role of grouping for road extraction. In: A. Gruen, E. Baltsavias and O. Henricsson (eds), Automatic Extraction of Man-Made Objects from Aerial and Space Images (II), Birkhäuser Verlag, Basel, Switzerland, pp. 245–256.

Taillandier, F., 2004. Reconstruction du bâti en milieu urbain: une approche multi-vues. PhD thesis, Ecole Polytechnique - Paris.

Vosselman, G., 2003. 3D reconstruction of roads and trees for city modeling. International Archives of Photogrammetry, Remote Sensing and Spatial Information Sciences XXXIV(part 3/W13), pp. 231–236.

Xu, G. and Z.Zhang, 1996. Epipolar geometry in stereo, motion and object recognition. Kluwer Academic Publishers.

Zhang, C., 2003. Updating of cartographic road databases by image analysis. PhD thesis, Institute of Geodesy and Photogrammetry, Zurich.